Preparation and characterization of Fe-based bulk metallic glasses in plate form

Preparation and characterization of Fe-based bulk metallic glasses in plate form

G.C. Lavorato [a,b], G. Fiore [b], A. Castellero [b], M. Baricco [b], J.A. Moya [c,d]

[a] INTECIN (FIUBA-CONICET), Paseo Colo´n 850, Capital Federal, Argentina [b] Dipartimento di Chimica IFM and NIS, Universita di Torino, Torino, Italy [c] IESIING, Facultad de Ingenierı´a e Informa´tica, UCASAL, Salta, Argentina [d] CONICET, Argentina

Abstract

Amorphous alloys with composition (at%) $Fe_{48}Cr_{15}Mo_{14}C_{15}B_6Gd_2$ (alloy A) and $Fe_{48}Cr_{15}Mo_{14}C_{15}B_6Y_2$ (alloy B) were prepared either using pure elements (A and B1) and a commercial AISI430 steel as a base material (B2). When prepared from pure elements both alloys (A and B1) could be cast in plate form with a fixed thickness of 2 mm and variable lengths between 10 and 20 mm by means of copper-mold injection in air atmosphere. In the case of alloy B2, prepared using commercial grade raw materials, rods of 2 mm diameter were obtained.

X-ray diffraction and scanning electron microscopy observations confirmed that an amorphous structure was obtained in all the as-cast samples. A minor fraction of crystalline phases (oxides and carbides) was detected on the as-cast surface. Differential scanning calorimetry measurements showed a glass transition temperature at 856 K for alloy A and 841 K for alloy B1, and an onset crystallization temperature of 887 K for alloy A and 885 K for alloy B1. In the case of alloy B2 a slightly different crystallization sequence was observed.

Values of hardness (13 GPa) and the Young modulus (180 GPa) were measured by nanoinden-tation for both the alloys.

The effects of adverse casting conditions (such as air atmosphere, non-conventional injection copper mold casting and partial replacement of pure elements with commercial grade raw materials) on the glass formation and properties of the alloy are discussed.

1. Introduction

Fe-based bulk metallic glasses (BMG), developed since 1995, show an interesting combination of physical and mechanical properties [1]. While conventional metallic glasses require rapid solidification with a cooling rate of about 10^6 K/s [2,3], BMGs can be formed at cooling rates between 1 and 100 K/s, leading to the possibility of casting much thicker objects [4]. At first, Fe-based BMGs were developed with the purpose of obtaining very good soft ferromagnetic properties due to the structural isotropy of the material (high Fe content alloys in Fe–B–Si system) [1,5]. How-ever, during the last decade, these materials could be prepared with lower Fe content showing a paramagnetic behavior at room temperature. These materials were named structural amorphous steels (SAS) [6,7] and today can be produced with a maximum thickness of 16 mm [8]. A number of interesting properties, such as the ability to be formed by thermoplastic processing in the supercooled liquid region, high strength, high hardness and excellent corrosion resistance, make these materials promising for engineering uses. However, in order to be employed as industrial materials, SASs still need to have larger toughness and lower fabrication costs that is currently high because of the use of pure elements and high vacuum conditions. Some attempts have been made to form bulk amorphous steels employing commercial-grade raw materials [9,10], conventional casting techniques and low vacuum conditions [11–13]. In this paper we have studied the effect of some processing conditions (air atmosphere, casting of a plate and use of commercial raw materials) on the glass formation and properties of two Fe-based BMGs.

2. Experimental

Samples with composition Fe48Cr15Mo14C15 B6Gd2 (alloy A) and Fe48Cr15Mo14C15 B6Y2 (alloy B1) were fabricated using pure elements. In order to evaluate the possibility of an industrial scale production of structural amorphous steels, the yttrium containing system (alloy B2) was also prepared using an AISI430 steel Gd2 O3 (55.7 wt%) and a commercial grade FeB alloy (7.3 wt.%) as base M23 (C.B)6 materials; the desired stoichiometry was obtained by adding Mo (25.7 wt%), C (3.4 wt%), Cr (5.4 wt%) and Y (3.4 wt%) in the form of pure elements. Master alloys were produced by arc-melting under (a.u.) Ar atmosphere. The samples were re-melted in an induction furnace and quenched in air atmosphere into a water-cooled intensity copper mold in order to obtain a glassy structure. A and B1 plates were produced using a mold with a rectangular cavity of width 20 mm and a fixed thickness of 2 mm. B2 alloy was cast in a rod shape using a cylindrical copper mold of 2 mm in diameter. Structural analysis was conducted by X-Ray diffraction (XRD) using the Philips XPert (Cu-Ka, λ=1.5418 A) and the Philips PW1830 (Co-Ka, λ=1.7897 A) diffractometers; the obtained patterns were plotted as a function of the wave vector S. The microstructure was examined in a Leica Stereoscan 4200 scanning electron microscope (SEM) and the chemical composition of the alloys was verified by means of Energy Dispersive Spectroscopy (EDS). Thermal analysis was performed in a Perkin Elmer Diamond differential scanning calorimeter (DSC) and in a Setaram high-temperature differential scanning calorimeter (HTDSC) at a heating rate of 0.17 K/s. Nanoindentation tests were carried out with a Fischerscope HM2000 employing a Vickers indenter. Several intensity indents were performed making sure that the maximum penetration displacement was significantly lower than 1/10 of the sample thickness. Values of indentation hardness (HIT) and elastic indentation modulus (EIT) were obtained from the loading and unloading curves, respectively, according to the procedure proposed by Oliver and Pharr [14].

3. Results and discussion

The as-cast surface of sample A, Fig. 1, exhibits the typical luster aspect of the metallic glass forming alloys. The diffraction patterns of samples A and B are shown in Fig. 2(a) and (b), respectively. In the case of samples A and B1, the XRD patterns of the as-cast surface of the plates (Fig. 2(a)-I and (b)-I, respectively) show the typical halo of the amorphous structure, together with some diffraction peaks corresponding to $M_{23}(B,C)_6$ and Y_2O_3/Gd_2O_3 phases. Similar observations have already been reported in similar Fe-based BMGs [13].

After removing a layer of about 0.1 mm from the outer surface, no crystalline diffraction peaks can be detected on the polished surfaces of samples A and B1 (Fig. 2(a)-II and (b)-II, respectively), indicating that the crystalline phases previously observed are mainly located on the surface. The formation of the crystalline phases at the surface can be likely attributed to the presence of oxygen contaminations in the casting atmosphere and to the presence of imperfections on the mold surface [15].

The XRD patterns of the cross-section of samples A and B1 (Fig. 2(a)-III and (b)-III, respectively) present a broad diffraction halo that is consistent with the presence of an amorphous structure. Nevertheless, it cannot be ruled out that the presence of small fraction of crystalline phases, mainly at the surface, could not be detected by XRD. In the case of alloys B2, XRD analyzes were conducted on slices cut transversally from the cylinder with respect to the casting direction and the XRD pattern does not present any crystalline diffraction peak, Fig. 2(b)-IV, indicating the presence of an amorphous structure.

The crystallization and melting curves obtained by high temperature DSC are shown in Fig. 3. The main characteristic temperatures and the thermal parameters describing the glass forming ability are listed in Table 1. For each sample it is possible to distinguish the glass transition followed by the crystallization exothermic signals; the glass transition event of alloy A was evidenced more clearly by means of conventional DSC, as shown in the inset of Fig. 3. The crystallization sequence of sample B2 appears to be different compared to one of sample B1: T_x is slightly higher and the crystallization of the amorphous phase occurs in two

exothermic peaks instead of the three observed in the case of sample B1. Furthermore, as reported in previous works [7,13,16,17], these alloys show an exothermic reaction at around 1200 K that could be interpreted as the transformation of a metastable $M_{23}(B,C)_6$ phase.

The thermograms of samples A and B1 reveal a non-eutectic melting, whereas B2 melts in a single endothermic peak followed by some high-temperature events that might be due to the melting of impurities present in the commercial grade raw materials. In the case of sample B2 the apparent liquidus temperature is significantly higher than the one observed for sample B1 leading to a decrease of the parameter $g¼T_x/(T_g\ þT_l)$ used for assessing the glass forming ability [18]. The maximum amorphous thickness achievable (critical casting thickness) is at least 2 mm in the case of B2 alloy. However, it is expected that the use of raw materials tends to reduce it with respect to the alloy prepared using pure elements. The reduction on the GFA can be inferred from differences in g parameter (0387 for B1 and 0380 for B2).

The SEM back-scattering micrograph of the cross-section taken from the top-middle part of sample A is shown in Fig. 4. It is possible to distinguish some micrometric sized precipitates that are homo-geneously distributed across the section. EDS chemical analysis revealed that the precipitates present very high fraction of Gd and O, while the surrounding amorphous matrix has less Gd content than expected. The same phenomenon was found for B1 and B2 alloys, where yttrium behaves in the same way as gadolinium. SEM results are in agreement with the detection of gadolinium and yttrium oxides from XRD patterns and confirm that they are formed not only on the surface but also inside the plate.

It is known that minor addition of rare earth elements (REs) is a powerful mean for modifying the properties and the glass forming ability of metallic glasses, and it was already employed in Fe-based BMGs [19]. The oxygen scavenging effect of REs is to retard the nucleation and growth of carbides, stabilizing the undercooled melt and, consequently, favoring the amorphization [6].

Nanoindentation tests were performed on the polished sur-faces of samples A and B1. The hardness and elastic modulus are reported in Table 1. Such values are in agreement with results previously reported for the same alloy prepared with pure ele-ments and conventional injection casting technique (H¼13 GPa, E¼180–200 GPa) [7] as well as for alloys with similar composition (H¼13.8 GPa) [6]. In addition, nanoindentation hardness values do not show significant variation across the sample suggesting that there are no local changes of composition and microstructure. Our results indicate that adverse casting conditions do not compromise the glass formation and the mechanical properties of the alloys studied in this work, and suggest that these alloys can be efficiently processed in view of applications where very high hardness is needed; however, the effect of the precipitates on the mechanical properties needs to be studied more in detail.

4. Conclusions

Three different Fe–Cr–Mo–C-based structural amorphous steels were successfully prepared with the purpose of contributing to the industrial development of this kind of alloys: i) they were all prepared in air atmosphere, ii) as an approach to near-net-shape fabrication two of them were obtained in a rectangular 2 mm thick plate shape, and iii) AISI 430 commercial steel was partially employed as raw material in the synthesis of the third alloy. The amorphous formation during quenching from the liquid state was promoted by minor alloying of Y and Gd, confirming previous studies. Minor alloying with REs was exploited to obtain successfully 2-mm-thick amor-phous plates, suggesting that the formation of crystalline phases can be avoided when the oxygen is removed from the melt by forming innocuous oxides. This seems to be a promising approach for the synthesis of BMGs starting from commercial grade raw materials in view of an industrial production. No major difference in neither structural nor thermal properties of both alloys was detected, but the thermal stability of the alloy made from commercial steel was significantly reduced. The structural and mechanical characteriza-tions are in agreement with the values previously reported in the literature. The results obtained in this work represent a promising step in view of the industrial application of this type of materials that could be employed in the future as biomedical instruments, die tools, sport goods and specific functional materials.

Acknowledgments

This work has been supported by the project PRIN-MIUR 2008B382JE_001.

References

[1] A. Inoue, Y. Shinohara, J.S. Gook, Mater. Trans. JIM 36 (1995) 1427.
[2] W. Klement, R.H. Willens, P. Duwez, Nature 187 (1960) 869.
[3] J.L. Walter, A.E. Berkowitz, Mater. Sci. Eng 67 (1984) 169.
[4] H.W. Kui, A.L. Greer, D. Turnbull, Appl. Phys. Lett. 45 (1984) 615.
[5] B. Shen, A. Inoue, J. Mater. Res. 19 (9) (2004).
[6] Z.P. Lu, C.T. Liu, J.R. Thompson, W.D. Porter, Phys. Rev. Lett. 92 (2004) 245503.
[7] V. Ponnambalam, S.J. Poon, G.J. Shiflet, J. Mater. Res. 19 (5) (2004) 1320.

[8] J. Shen, Q. Chen, J. Sun, H. Fan, G. Wang, Appl. Phys. Lett. 86 (2005) 151907.
[9] J. Cheney, K. Vecchio, Mater. Sci. Eng. A 492 (2008) 230.
[10] Y.H. Zhao, C.Y. Luo, X.K. Xi, D.Q. Zhao, M.X. Pan, W.H. Wang, Intermetallics 14 (2006) 1107.
[11] A. Bouchareb, B. Bendjemil, R. Piccin, M. Baricco, Int. J Nanoelectronics Mater. 3 (2010) 63.
[12] A. Bouchareb, B. Bendjemil, R. Piccin, M. Baricco, Chin. Phys. Lett. 27 (2010) 076103.
[13] J. Pan, Q. Chen, N. Li, L. Liu, J. Alloys Compd. 463 (2008) 246.
[14] W.C. Oliver, G.M. Pharr, J. Mater. Res. 7 (1992) 1564.
[15] M.J. Kramer, H. Mecco, K.W. Dennis, E. Vargonova, R.W. McCallum, R.E. Napolitano, J. Non-Cryst. Solids 353 (2007) 3633.
[16] T.A. Baser, M. Baricco, J. Alloys Compd. 176 (2007) 434.
[17] T.A. Baser, M. Baricco, S. Enzo, G. Vaughan, A.R. Yavari, J. Mater. Res. 23 (2008) 2166.
[18] Z.P. Lu, C.T. Liu, Acta Mater. 50 (2002) 3501.
[19] W.H. Wang, Prog. Mater. Sci. 52 (2007) 540.

FIGURES AND TABLES

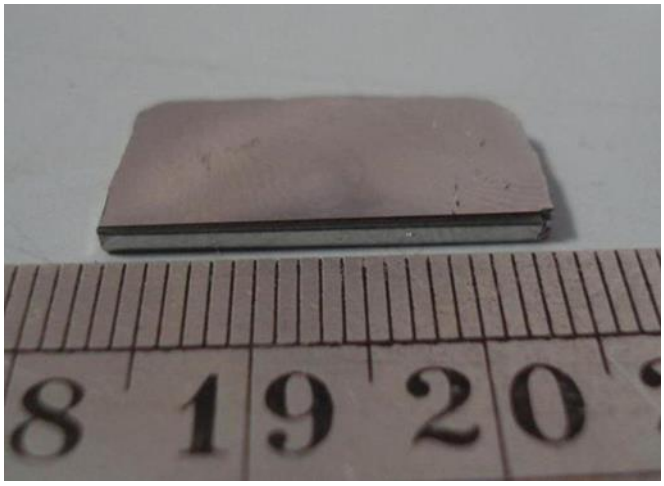

Fig. 1. Outer aspect of $Fe_{48}Cr_{15}Mo_{14}C_{15}B_6Gd_2$ amorphous plate.

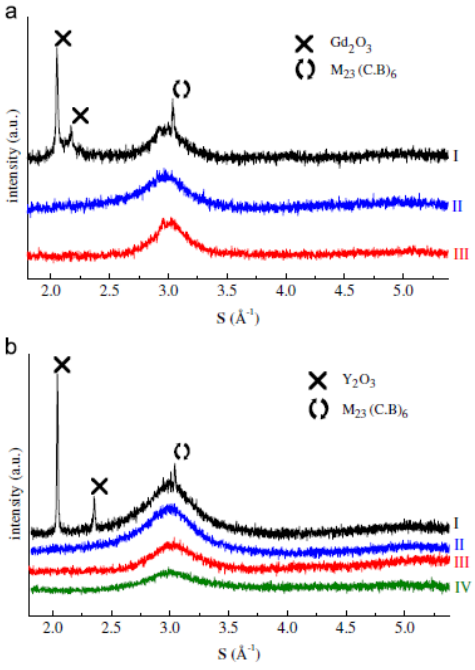

Fig. 2. (a) X-ray diffraction patterns of alloy A: as-cast surface (I), polished surface (II), cross-section (III); (b) X-ray diffraction patterns of alloy B: B1 as-cast surface (I), B1 polished surface (II), B1 cross-section (III), B2 cross-section (IV).

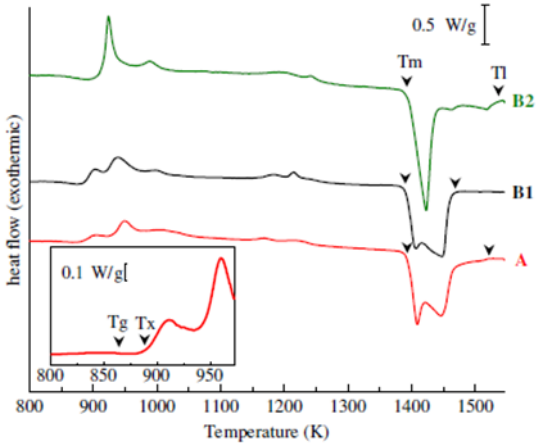

Fig. 3. HTDSC and DSC (inset) curves measured at a heating rate of 0.17 K/s.

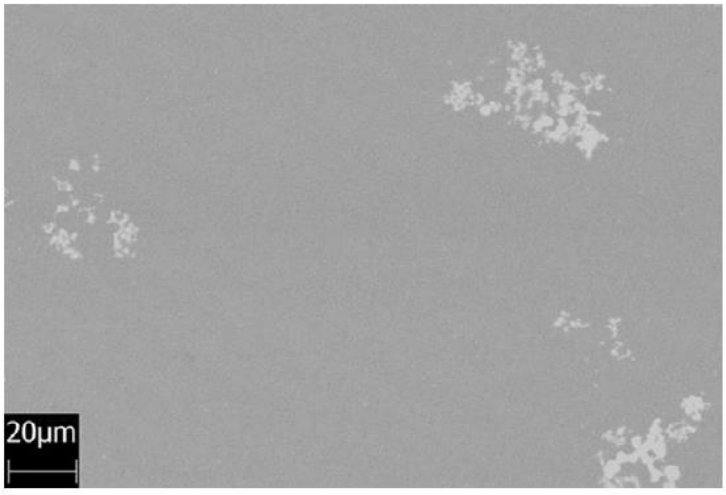

Fig. 4. SEM back-scattering image of the as-cast $Fe_{48}Cr_{15}Mo_{14}C_{15}B_6Gd_2$ BMG.

Table 1
Thermal and mechanical properties of samples A, B1 and B2.

	T_g (K)	T_x (K)	T_m (K)	T_l (K)	c	H (GPa)	E (GPa)
A	856	887	1393	1519	0.373	13.370.3	18375
B1	841	885	1389	1460	0.386	13.140.4	174723
B2	848	903	1395	1528	0.380	–	–